The Journal of Clinical Endocrinology & Metabolism, 2022, **107**, 1346–1356
https://doi.org/10.1210/clinem/dgab932
Advance access publication 31 December 2021
Clinical Research Article

PNC2 (*SLC25A36*) Deficiency Associated With the Hyperinsulinism/Hyperammonemia Syndrome

Maher A. Shahroor,[1,2,*] Francesco M. Lasorsa,[3,4,*] Vito Porcelli,[3] Imad Dweikat,[5] Maria Antonietta Di Noia,[3] Michal Gur,[6] Giulia Agostino,[3] Avraham Shaag,[6] Teresa Rinaldi,[7] Giuseppe Gasparre,[8] Flora Guerra,[8] Alessandra Castegna,[3,4] Simona Todisco,[3] Bassam Abu-Libdeh,[1] Orly Elpeleg,[6] Luigi Palmieri,[3,4]

[1]Department of Pediatrics and Genetics, Al Makassed Hospital and Al-Quds University, 95908 Jerusalem, Palestine
[2]Department of Neonatology, Sunnybrook Health Sciences Center, University of Toronto, M4N 3M5 Toronto, Canada
[3]Laboratory of Biochemistry and Molecular Biology, Department of Biosciences, Biotechnologies and Biopharmaceutics, University of Bari Aldo Moro, 70125 Bari, Italy
[4]CNR Institute of Biomembranes, Bioenergetics and Molecular Biotechnologies, 70125 Bari, Italy
[5]Metabolic Unit, An-Najah National University, P467 Nablus, Palestine
[6]Department of Genetics, Hadassah, Hebrew University Medical Center, 91120 Jerusalem, Israel
[7]Pasteur Institute-Cenci Bolognetti Foundation, Department of Biology and Biotechnology "Charles Darwin", University of Rome La Sapienza, 00185 Rome, Italy
[8]Department of Medical and Surgical Sciences (DIMEC), Unit of Medical Genetics and Center for Applied Biomedical Research (CRBA), University of Bologna, 40138 Bologna, Italy

Correspondence: Prof. Orly Elpeleg, Department of Genetics, Hadassah, Hebrew University Medical Center, Jerusalem, Israel. Email: elpeleg@hadassah.org.il; or Prof. Luigi Palmieri, University of Bari Aldo Moro, Bari, Italy. Email: luigi.palmieri@uniba.it.
*M.A.S. and F.M.L. contributed equally

Abstract

Context: The hyperinsulinism/hyperammonemia (HI/HA) syndrome, the second-most common form of congenital hyperinsulinism, has been associated with dominant mutations in *GLUD1*, coding for the mitochondrial enzyme glutamate dehydrogenase, that increase enzyme activity by reducing its sensitivity to allosteric inhibition by GTP.

Objective: To identify the underlying genetic etiology in 2 siblings who presented with the biochemical features of HI/HA syndrome but did not carry pathogenic variants in *GLUD1*, and to determine the functional impact of the newly identified mutation.

Methods: The patients were investigated by whole exome sequencing. Yeast complementation studies and biochemical assays on the recombinant mutated protein were performed. The consequences of stable *slc25a36* silencing in HeLa cells were also investigated.

Results: A homozygous splice site variant was identified in solute carrier family 25, member 36 (*SLC25A36*), encoding the pyrimidine nucleotide carrier 2 (PNC2), a mitochondrial nucleotide carrier that transports pyrimidine as well as guanine nucleotides across the inner mitochondrial membrane. The mutation leads to a 26-aa in-frame deletion in the first repeat domain of the protein, which abolishes transport activity. Furthermore, knockdown of *slc25a36* expression in HeLa cells caused a marked reduction in the mitochondrial GTP content, which likely leads to a hyperactivation of glutamate dehydrogenase in our patients.

Conclusion: We report for the first time a mutation in PNC2/SLC25A36 leading to HI/HA and provide functional evidence of the molecular mechanism responsible for this phenotype. Our findings underscore the importance of mitochondrial nucleotide metabolism and expand the role of mitochondrial transporters in insulin secretion.

Key Words: hyperinsulinism/hyperammonemia syndrome, mitochondrial carrier, SLC25A36, PNC2, nucleotide metabolism, GTP

Abbreviations: AGC1, aspartate/glutamate carrier isoform 1; DAPI, 4′,6-diamidino-2-phenylindole; GDH, glutamate dehydrogenase; *GLUD1*, mitochondrial glutamate dehydrogenase gene; HI/HA, hyperinsulinism/hyperammonemia syndrome; KATP, ATP-sensitive potassium channel; LC-MS/MS, liquid chromatography–tandem mass spectrometry; PCR, polymerase chain reaction; PNC2, pyrimidine nucleotide carrier 2; qPCR, quantitative polymerase chain reaction; *SLC25A36*, gene encoding pyrimidine nucleotide carrier 2; TMRM, tetramethyl rhodamine methyl ester; WES, whole exome sequencing; WT, wild-type.

Hyperinsulinemic hypoglycemia is a rare form of hypoglycemia in childhood. Within this group, hyperinsulinism/hyperammonemia syndrome (HI/HA, OMIM: 606762), is an important etiology due to autosomal dominant inheritance of de novo mutations in *GLUD1* coding for the mitochondrial enzyme glutamate dehydrogenase (GDH). Most pathogenic mutations in *GLUD1* make GDH unresponsive to the allosteric inhibition by mitochondrial GTP, with the consequent upregulation of the insulin secretion (1). The major clinical feature of children with the HI/HA syndrome is recurrent episodes of symptomatic hypoglycemia which may occur with fasting but can also be provoked by protein feeding (1). Unlike infants with hyperinsulinism due to defects of the ATP-sensitive K^+-channel (KATP) channel (mutations of SUR1 or

Received: 12 August 2021. **Editorial Decision:** 29 December 2021. **Corrected and Typeset:** 19 January 2022

Kir6.2), HI/HA patients are born with a normal birth weight and their hypoglycemia is milder, hence often not recognized until several months of age (2). The hyperammonemia is persistent, asymptomatic, and mild, (2-5 times the upper limit of normal), it is associated with normal plasma amino acid levels, and it is not altered by dietary intake, glucose levels, or treatment with sodium benzoate, phenylacetate, or carbamoylglutamate.

Here, we report the case of 2 siblings who presented a clinical phenotype compatible with the HI/HA syndrome with protein-related hypoglycemia and persistent mild hyperammonemia, that was not associated with *GLUD1* mutations. The patients underwent whole exome sequencing (WES) analysis that revealed a rare, deleterious homozygous variant in the *SLC25A36* gene encoding a defective mitochondrial pyrimidine nucleotide carrier 2 (PNC2) (3), a member of the mitochondrial carrier family (4). PNC2 impairment likely leads to a reduced mitochondrial GTP content, hence limiting GDH inhibition and hyperactivating insulin secretion pathway.

Methods

Patients and Clinical Data

We investigated a consanguineous Palestinian family (see pedigree, Fig. 1A) including 2 affected siblings who presented a clinical phenotype compatible with the HI/HA syndrome with protein-related hypoglycemia and persistent mild hyperammonemia. Contributing investigators provided clinical information on affected children and their family. This study was approved by the ethical committees of Hadassah Medical Center and the Israeli Ministry of Health, and written informed consent was obtained from subjects or their parents.

Whole Exome Sequencing

Exonic sequences from a DNA sample of patient II-3 were enriched with the SureSelect Human All Exon 50 Mb V.4 Kit (Agilent Technologies, Santa Clara, California, USA). Sequences (100-bp paired-end) were generated on a HiSeq2500 (Illumina, San Diego, California, USA). Read alignment and variant calling were performed with DNAnexus (Palo Alto, California, USA) using default parameters with the human genome assembly hg19 (GRCh37) as reference. Parental consent was given for genetic studies. The study was performed with the approval of the ethical committees of Hadassah Medical Center and the Israeli Ministry of Health.

Expression Analysis by Real-Time Polymerase Chain Reaction

Total RNA from normal human tissues (Ambion) was reverse-transcribed with GeneAmp RNA PCR Core kit (Applied Biosystems) with random hexamers as primers. The quantitative polymerase chain reaction (qPCR) reactions were performed using an ABI Prism 7900 HT (Applied Biosystems). TaqMan-MGB Probe and primers based on the cDNA sequences of *SLC25A33* (Assay ID: Hs00757629_s1) and *SLC25A36* (Assay ID: Hs00216785_m1) were purchased from Applied Biosystems. To correct for differences in the amount of starting first-strand cDNAs, the human peptidylprolyl isomerase A (*PPIA*) gene was amplified in parallel (assay ID: Hs99999904_m1) as a reference gene (5). The relative quantification of mRNA for *SLC25A33* and *SLC25A36* was performed according to the comparative method ($2^{-\Delta\Delta Ct}$) (6), where ΔCt of the liver was chosen as calibrator.

Construction of Expression Plasmids

The coding sequence of *SLC25A36* (NM_00114647.1) was used as template for the deletion of 78 nucleotides (from G208 to A285) coding for 26 amino acids (from V70 to R95) found in the patients through WES. Briefly, 2 fragments of the template DNA were amplified by PCR using 2 external primers (A and D) corresponding to the extremities of the *SLC25A36* coding sequence, with additional BamHI (A: 5′-aaaGGATCC atgagccagagggacacgct-3′) and EcoRI (D: 5′-aaaGAATTCctat ccattgagtaggtaaacc-3′) restriction sites, and 2 internal primers (B and C) corresponding to the flanking regions of the target DNA sequence to be deleted, with additional complementary sequences (15 nucleotides) at their 3′ ends (B: 5′-AGCAAA GTATATTGCctttaggcaatgaag-3′; C: 5′-cttcattgcctaaagGCAA TATACTTTGCT-3′). The 2 overlapping fragments obtained (AB and CD) were used as template for a second PCR using the external primers A and D to obtain the coding sequence of *SLC25A36* devoid of the deleted region. The amplified

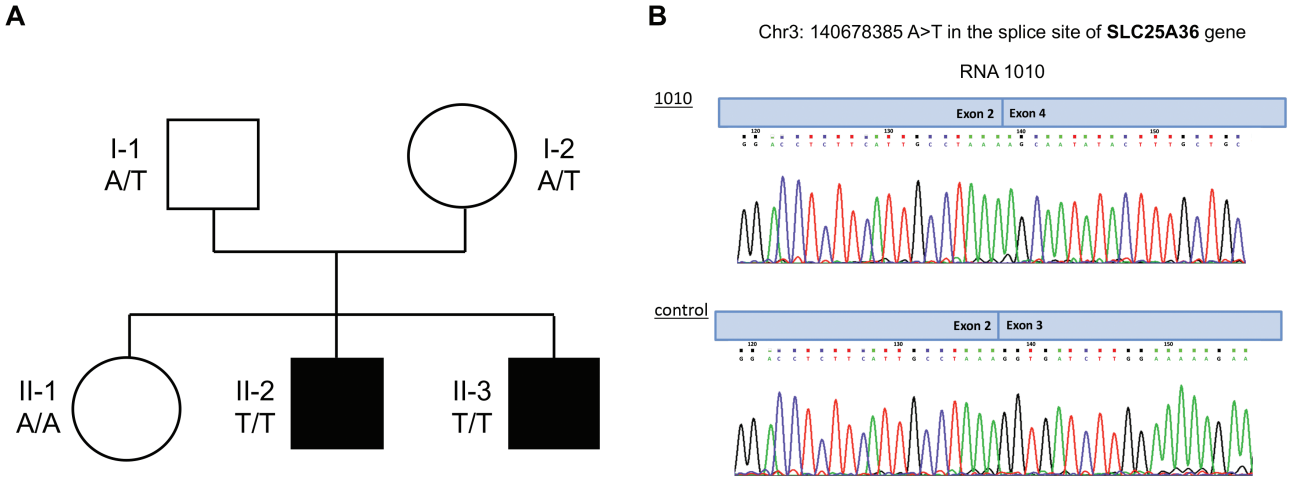

Figure 1. (A) Family pedigree and genotype. Filled symbols denote affected individual. (B) *SLC25A36* cDNA sequence around the mutation site. Patient cDNA in the upper panel showing exon 3 skipping, control cDNA in the lower panel.

product was BamHI/EcoRI digested and inserted into the pMWT7 vector for the expression in *E. coli* (3). A similar approach was used to clone the mutated *SLC25A36* coding sequence, *SLC25A36 Δ* 36, into the pRS42H plasmid except that HindIII (primer E in the place of primer A: 5′-AAAaagct tGTTCTTTATTCTGACCTATATAG-3′) and BamHI (primer F in the place of primer D: 5′-AAAggatccTCACAGGGGAAA AGCCCAT-3′) restriction sites were used for the ligation and the *SLC25A36*-pRS42H expression vector (3) as template.

Bacterial Expression, Reconstitution of Recombinant Proteins Into Liposomes and Transport Assays

The recombinant wild-type (WT) and mutated SLC25A36 were expressed in *E. coli* BL21(DE3) and purified, as previously described (3). Then 30 µg of the recombinant proteins were solubilized with 1.2% (w/v) lauric acid and incorporated into liposomes in the presence of 1% (w/v) TX-114 and 10mM CTP, pH 6.25 with the Amberlite (Merck) method (7). Virtually identical amounts of incorporated proteins in the proteoliposomes (16%-20% of the protein added to the reconstitution mixture) were obtained for all variants tested. For the transport assays, the external substrate was removed from proteoliposomes on Sephadex G-75 columns and transport at 25 °C was started by adding 0.2mM [^{3}H]-CTP to proteoliposomes. The transport assays were terminated by the addition of 30mM pyridoxal-5′-phosphate and 20mM bathophenanthroline after 3 minutes within the initial rate of substrate uptake (3). In controls, the inhibitors were added at time 0. Finally, the external radioactivity was removed with a Sephadex G-75 column and the entrapped [^{3}H]-CTP was measured by subtracting the control values.

SLC25A36 Silencing in HeLa Cells

The shRNA cassette 5′-TCTATAATCTGCTTTGCTATCTC GAGATAGCAAAGCAGATTATAGTTTTT-3′ was designed as a hairpin-loop structure based on the *SLC25A36* cDNA sequence according to the guidelines described in http://sirna.wi.mit.edu/ (8) and AgeI/EcoRI cloned into the pLKO.1 vector, as previously described (9). The resulting construct (pLKO-siA36) was used for the recombinant generation of lentiviral particles (LVshA36) with the Lentiviral Packaging Mix (Sigma) in HEK293T. HeLa cells cultured at 37 °C at 5% CO_2 in high glucose DMEM (Sigma) supplemented with 10% fetal bovine serum, were transduced with recombinant lentivirus at viral titer of ~5 plaque-forming units/mL for 24 hours at 37 °C and selected in the presence of 5 µg/mL puromycin. A lentiviral construct carrying a mismatch shRNA (LVshMM) (9) was used at the same titer to select control cells. The efficiency of *SLC25A36* silencing in puromycin selected cells was estimated by RealTime qPCR.

Quantification of Mitochondrial Nucleotide Content

Cells were detached from flasks by trypsinization, resuspended in ice in a cold ipotonic buffer (0.5 mM $MgCl_2$, 2.5 mM NaCl, 3.5 mM Tris-HCl, pH 7.8) and mitochondria isolated by using a glass Potter-Elvehjem homogenizer and serial centrifugations, as previously described (10). The mitochondrial pellet was resuspended in 0.32M sucrose, 1mM EDTA, and 10mM Tris-HCl and its protein content assayed by Bradford method. To estimate mitochondrial nucleotides content, isolated mitochondria were suspended in 70% (v/v) cold methanol, centrifuged, and kept at –80 °C overnight. Samples were then lyophilized, redissolved in water, recentrifuged, and filtered before electrospray ionization (ESI) liquid chromatography–tandem mass spectrometry (LC-MS/MS) analysis using an Acquity UPLC system coupled to a Quattro Premier mass spectrometer (Waters, Milford, MA, USA). Separation was achieved using a HSST3 C18 column (2.1 × 50 mm, 1.7 µm particle size; Waters) eluted (0.3 mL/min) with a linear gradient from 100% 50mM ammonium acetate to 10% 50mM ammonium acetate/90% acetonitrile (11). Calibration curves for standards processed under the same conditions as samples were used for quantification. Nucleotide standard solutions were used to validate peak positions.

Mitochondrial DNA Content and Sequencing

Total DNA was isolated from HeLa cells using the GenEluteTM Mammalian Genomic DNA Miniprep kit (Sigma). The content of mtDNA relative to nuclear DNA was measured by Real-Time qPCR following amplification of mtND1 gene and the reference ACTB nuclear gene. The method was validated by evaluating the equal reaction efficiency of the 2 amplicons. Each sample was analyzed in triplicate in 3 to 4 different experiments. The average difference in threshold cycle values (ΔCt, namely CtND1—CtActin) was used as a measure of the abundance of the mitochondrial genome relative to the nuclear genome. In particular, the mtDNA/nDNA ratio is reported as $2^{-\Delta Ct}$. Total DNA (1 ng) was used for the amplification of mtDNA with the MitoALL Resequencing kit in a final volume of 10 µL using a 9700 thermal cycler following the conditions given by the manufacturer (Applera). PCR products were purified by digestion with 10 units of EXOSAPit (U.S. Biochemical) at 37 °C for 30 minutes, followed by heat inactivation at 80 °C for 15 minutes. The PCR product (5-10 ng) was used for direct sequencing with BigDye kit version 1.1 (Applera). Sequences were run in the ABI 3730 Genetic Analyzer automated sequencing machine. Electropherograms were analyzed with Sequencing Analysis version 2.5.1 software and inspected with SeqScape version 2.5 software (Applera) (12). Prediction of pathogenic potential of missense mutations was performed with PolyPhen2 (13), as previously described (12).

Fluorescence Imaging

For fluorescence microscopic analyses of *Saccharomyces cerevisiae*, cells were grown in YPD at 28 °C, then exponential phase cells were fixed with 1% formaldehyde and treated with 1 µg/mL for 4,6-diamidino-2-phenylindole (DAPI; Sigma) staining. The fluorescence (exc 365 nm; emis 450nm) was observed using a Zeiss Axio Imager Z1 Fluorescence Microscope with 63× oil objective and the AxioVision 4.8 Digital Image Processing System. Mitochondrial membrane potential (Δψm) of HeLa cells was measured by loading the cells with 20nM tetramethyl rhodamine methyl ester (TMRM, Thermofisher) for 30 minutes at 37 °C. Images were taken on an inverted Zeiss Axiovert 200 microscope with 40× oil objective equipped with Photometrics Cascade 512 CCD-camera (Roper Scientific, USA) and elaborated with the software Metafluor 6.1 (Universal Imaging Co., USA). TMRM intensities (exc 560 nm; emis 590-650 nm) were imaged every 10 seconds with a fixed 20-ms exposure time. At the end of the experiments, 1 µM FCCP was added after 180 acquisitions to collapse the Δψµ and to subtract the

nonmitochondrial TMRM fluorescence. Mitochondrial mass of HeLa cells was determined by incubating the cells with 100nM MitoTrackerGreen (Thermofisher) for 30 minutes at 37 °C at 5% CO_2. The green fluorescence intensity of the probe that marks the mitochondria independently of $\Delta\psi m$ was measured by using Tali Image Cytometer (Thermofisher).

Yeast Strains and Growth Conditions

Strains were grown at 28 °C (unless otherwise indicated) in rich medium containing 1% Bacto-peptone and 1% yeast extract supplemented with 2% glucose (YPD) or 3% glycerol (YPG). 2.2% Bacto agar (Difco) was also present in solid media. In all cases the final pH was adjusted to 4.5. The *RIM2 Δ* haploid strain was generated by homologous recombination of the kanMX cassette at the *RIM2* gene locus in the wild-type W303 strain (*his3-11,15; ade2-1; leu2*-3,112; ura3-1; trp1-1; can1-100), as previously described (3). To obtain *RIM2 Δ* strains containing mtDNA, the *RIM2 Δ* haploid strain was crossed with the wild-type haploid strain transformed with either the *SLC25A36 WT*-pRS42H or the *SLC25A36 Δ* 36-pRS42H plasmid and all the transformed *RIM2/RIM2* Δ diploid strains selected were streaked on YPD plates containing 100 µg/mL hygromycin for plasmid maintenance. Sporulation and the tetrads dissection were carried out as previously described (3). After 3 days on YPD, tetrad analysis was performed using marker selection; *RIM2* Δ spores were Geneticin (G418)-resistant; transformed spores (both WT *RIM2* and *RIM2*Δ) were hygromycin-resistant.

Results

Clinical Case Reports

The index case, patient II-3 in Fig. 1A, was a 5-year-old boy, the third child born to second-degree cousins of Palestinian origin. The pregnancy, delivery, and early development were uneventful but since several months of age he presented with daily episodes of generalized tonic clonic movements, cyanosis, and frothy mouth secretions. The patient was treated with benzodiazepam or intravenous glucose but some of the attacks resolved spontaneously after a couple of minutes. The attacks were mostly associated with very low levels of blood glucose (peak 16 mg%, N > 70), high insulin levels (peak level during hypoglycemia 59.3 µU/mL, normal fasting level < 17), high C-peptide (peak 5.2 ng/mL, N < 3.3), high ammonia (peak level 283 µM, 29 < N < 70), and normal levels of blood gas, urine organic acids, serum amino acids, insulin, lactic acid, thyroid functions, cortisol, and growth hormone, with trace serum ketones, and normal total and free carnitine and acylcarnitine profile. Between episodes, blood glucose was normal, but ammonia level was still high. Protein load was performed at 2 years of age: blood glucose at baseline was 85 mg% but dropped to 30 mg% at 120 minutes. After 2 years of age, normal glucose levels were frequently documented even during attacks, for which the patient was kept on Tegretol. At 4 years of age, growth parameters were normal (weight 20 kg, 70th percentile; height 105 cm, 20th percentile; and head circumference 49 cm, 10th percentile). The physical examination was normal as was his psychomotor and social development.

Patient II-2 (Fig. 1A), the second child in the family, was a 6-year-old male. At 8 months of age, he experienced recurrent attacks of a similar nature. They were associated with hypoglycemia and hyperammonemia and were usually preceded by a meal which included protein, not necessarily a high protein load. The attacks were abated by low-protein diet; sodium benzoate was additionally administered. At 6 years, his development was age-appropriate, and the physical examination was normal, but he had short stature (weight 18.5 kg, 20th percentile; length 95 cm, 0.1st percentile).

Additional testing included muscle biopsy, which revealed normal enzymatic activities of the 5 mitochondrial respiratory chain complexes, and sequence determination of coding exons of *GLUD1* and *SUR1* which did not disclose any rare, pathogenic variant in both siblings.

The parents and the sister, II-1(Fig. 1A), were healthy.

Mutation Analysis

Given the consanguinity in this family, we performed WES under the hypothesis of a recessively inherited, rare, causal allele. WES of patient II-3 yielded 46.5 million mapped reads with a mean coverage of X94. Following alignment and variant calling, we performed a series of filtering steps. These included removing variants which were called less than X8, were off-target, heterozygous, synonymous, had minor allele frequency (MAF) > 0.5% or homozygotes at gnomAD (Genome Aggregation database, (https://gnomad.broadinstitute.org/)), MAF > 2% at the Hadassah in-house database (~2500 ethnic matched exome analyses).

Seven variants survived this filtering (Table 1) but after genotyping family members by Sanger sequencing and considering codon conservation and variant pathogenicity scores, we focused on hg19:Chr.3: 140678385 A > T, rs1027790661 c.284 + 3 A > T in *SLC25A36*. This variant was absent from the ~ 35 250 exome/genome analyses of healthy individuals which covered this genomic position and were deposited at

Table 1. Homozygous variants retained after variant filtering of exome analysis

Chr	bp (Hg19)	HGVSc	HGVSp	dbsnp	Gene
2	71741038	c.746C > T	p.Pro249Leu	rs147876220	DYSF
12	103699848	c.535T > C	p.Ser179Pro		C12orf42
3	140275379	c.1699A > G	p.Ile567Val	rs199944362	CLSTN2
12	101731990	c.3803C > T	p.Thr1268Ile	rs752232067	UTP20
2	97039065	c.2202T > A	p.Asp734Glu	rs139592813	NCAPH
9	312083	c.658G > A	p.Glu220Lys	rs373168547	DOCK8
3	140678385	c.284 + 3A > T		rs1027790661	**SLC25A36**

Bp(Hg19), genomic position in human genome assembly. GRCh37, HGVSc-human genome variation society coding sequence name. HGVSp, human genome variation society protein sequence name.

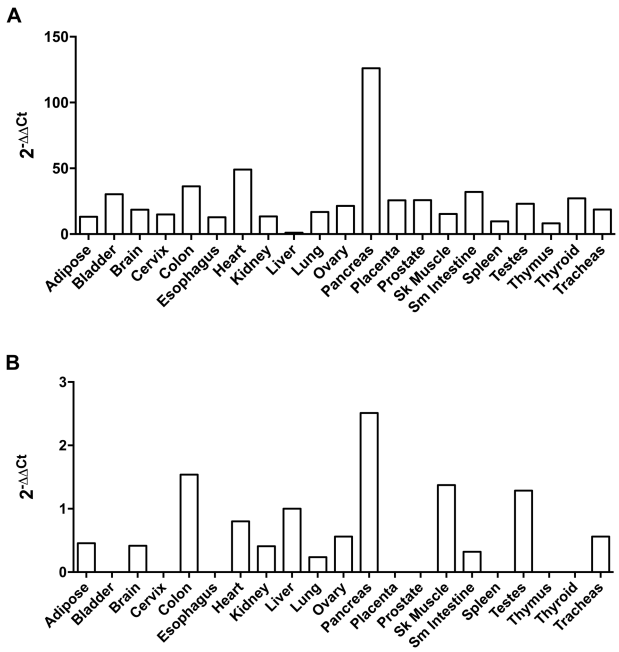

Figure 2. Expression of *SLC25A36* and *SLC25A33* in various tissues. The relative expression of *SLC25A36* (A) and *SLC25A33* (B) gene was quantified by qPCR according to the comparative method ($2^{-\Delta\Delta Ct}$) in the indicated tissues. ΔCt values were calculated using human peptidylprolyl isomerase A (PPIA) gene as reference gene. For the internal calibrator (liver), ΔΔCt = 0, and $2^0 = 1$. For the different tissues, the value of $2^{-\Delta\Delta Ct}$ indicates the fold change in mRNA values relative to the calibrator.

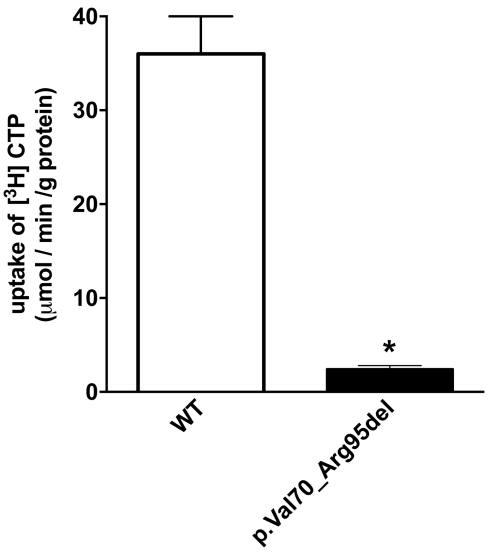

Figure 3. Functional analysis of wild-type (WT) and mutated SLC25A36 forms. (A) The uptake rate of [^{3}H]-CTP was measured by adding 0.2 mM of [^{3}H]-CTP to proteoliposomes reconstituted with similar amount of purified wild-type or mutated SLC25A36 recombinant protein. The proteoliposomes were preloaded internally with 10 mM of CTP. The means and SDs from 5 independent experiments are shown $^*P < 0.01$, one-way *t* test analysis.

gnomAD database and segregated with the disease in family (Fig. 1A). To find the effect of the variant on *SLC25A36* transcription, we generated cDNA from the patient lymphocytes and noted homozygous exon 3 skipping (Fig. 1B) with loss of 26 amino acids (V70 till R95) in the first repeat of the protein.

SLC25A36 Expression Analysis

SLC25A36 encodes for PNC2, a mitochondrial carrier for cytosine and uracil (deoxy)nucleotides as well as (d)GNPs (3). To investigate its expression in various human tissues, real-time PCR analyses were performed on total RNA populations using primers and probes specific for *SLC25A36* and for its closest homologue *SLC25A33* encoding the pyrimidine nucleotide carrier 1 (PNC1), which was shown to transport uracil, thymine, and cytosine (deoxy)-nucleoside di- and triphosphates (3, 14). With the exception of liver, where *SLC25A36* and *SLC25A33* transcripts have similar threshold cycle value (Fig. 2), the SLC25A36 mRNA levels (Fig. 2A) were higher than the *SLC25A33* mRNA levels in the investigated tissues (Fig. 2B). SLC25A36 was expressed most strongly in pancreas, where its transcript levels were more than 30-fold higher than those of *SLC25A33* (Fig. 2), suggesting a major role of PNC2 in this tissue.

Functional Analysis of the SLC25A36 Mutation

In order to study the effect of the deletion found in the patients on PNC2 transport activity, WT and mutated proteins were expressed in *Escherichia coli*, purified, and reconstituted into liposomes to monitor the activity of PNC2. As shown in Fig. 3, the deletion caused a strong reduction of nucleotide transport catalyzed by PNC2.

To investigate the physiological relevance of PNC2 activity impairment, we evaluated the nucleotide content in mitochondria of HeLa cells stably transduced with a lentiviral construct carrying a shRNA sequence silencing *SLC25A36*. Two distinct puromycin-resistant cultures (LVshA36-HeLa.1 and LVshA36-HeLa.2) were selected, both with about 60% reduction of *SLC25A36* mRNA levels, as compared with control cells stably transduced with a lentivirus containing a mismatch shRNA sequence (LVshMM-HeLa) (Fig. 4A). In bright field and fluorescence microscopy, LVshA36-HeLa.1 and LVshA36-HeLa.2 cells did not reveal evident changes in cell size and morphology (not shown), and TMRM-stained mitochondria appeared not significantly different from that of LVshMM-HeLa cells, in terms of both morphology and membrane potential (Fig. 4B). As measured by LC-MS/MS, in mitochondria isolated from both LVshA36-HeLa.1 and LVshA36-HeLa.2 cells, CTP and GTP levels were significantly lower than those measured in control LVshMM-HeLa cells (Fig. 5A and 5B), in keeping with a reduced transport activity of PNC2 (3). By contrast, no significant differences were measured in the intramitochondrial content of other nucleoside triphosphates, such as UTP, TTP (Fig. 5C and 5D), and ATP (not shown), most likely due to the presence of PNC1 that displays a substrate preference for U and T nucleotides. Accordingly, it has been previously reported that mitochondrial UTP levels were significantly reduced in SLC25A33/pnc1 siRNA-transfected MCF-7 cells, whereas GTP as well as ATP levels were not significantly altered (15).

Interestingly, cells with suppressed PNC1 displayed reduced mtDNA (15). Indeed, a significant reduction of mtDNA content was revealed in *SLC25A36*-silenced cells as compared with control cells (Fig. 5E) but no alteration of mtDNA sequence. The fluorescence of LVshA36-HeLa.1 and LVshA36-HeLa.2 mitochondria marked with MitoTrackerGreen was increased by about 20% as compared with that measured in LVshMM-HeLa cells (Fig. 5F), indicating an increase of mitochondrial biogenesis associated with PNC2 downregulation. This observation, that resembles what already described in

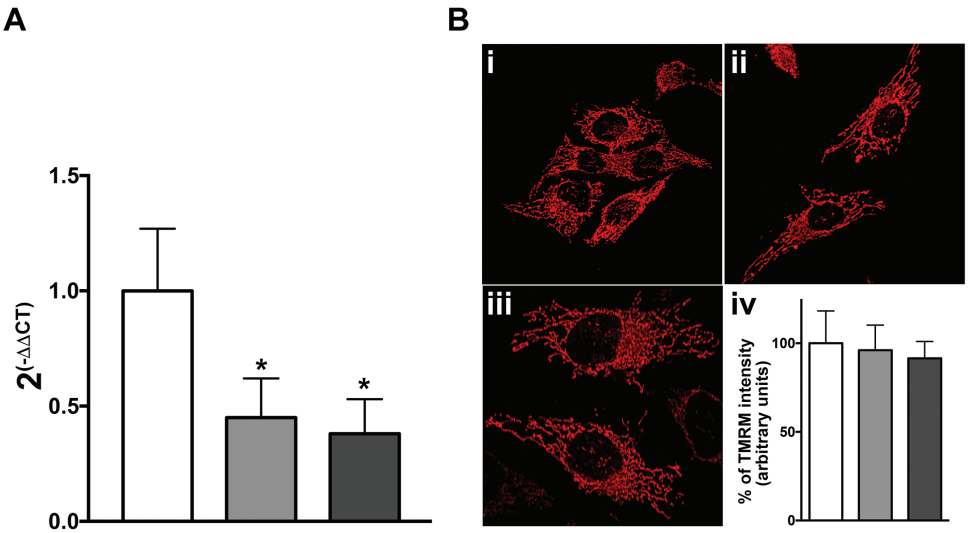

Figure 4. Downregulation of *SLC25A36* gene in HeLa cells. (A) Relative expression of *SLC25A36* gene in HeLa cells infected with LVshMM (white column) or LVshA36 (gray and dark gray column, 2 independent cultures) lentiviral particles and selected in the presence of puromycin 1 μg/mL. Data are the means ± SD from 3 independent qRT measurements. *$P < 0.01$ one-way analysis with Bonferroni *t* test. (B) $\Delta\psi m$ were measured by fluorescence microscopy in LVshMM-HeLa (panel i and white column), LVshA36-HeLa.1 (panel ii and gray column) and LVshA36-HeLa.2 (panel iii and dark gray column) cells loaded with 20 nM TMRM for 30 minutes at 37 °C and fluorescence intensities were imaged every 5 seconds with a fixed 20-ms exposure time. Data of panel iv are the means ± SD of TMRM percentage intensities normalized to values measured after addition of 1 μM FCCP in 3 independent experiments.

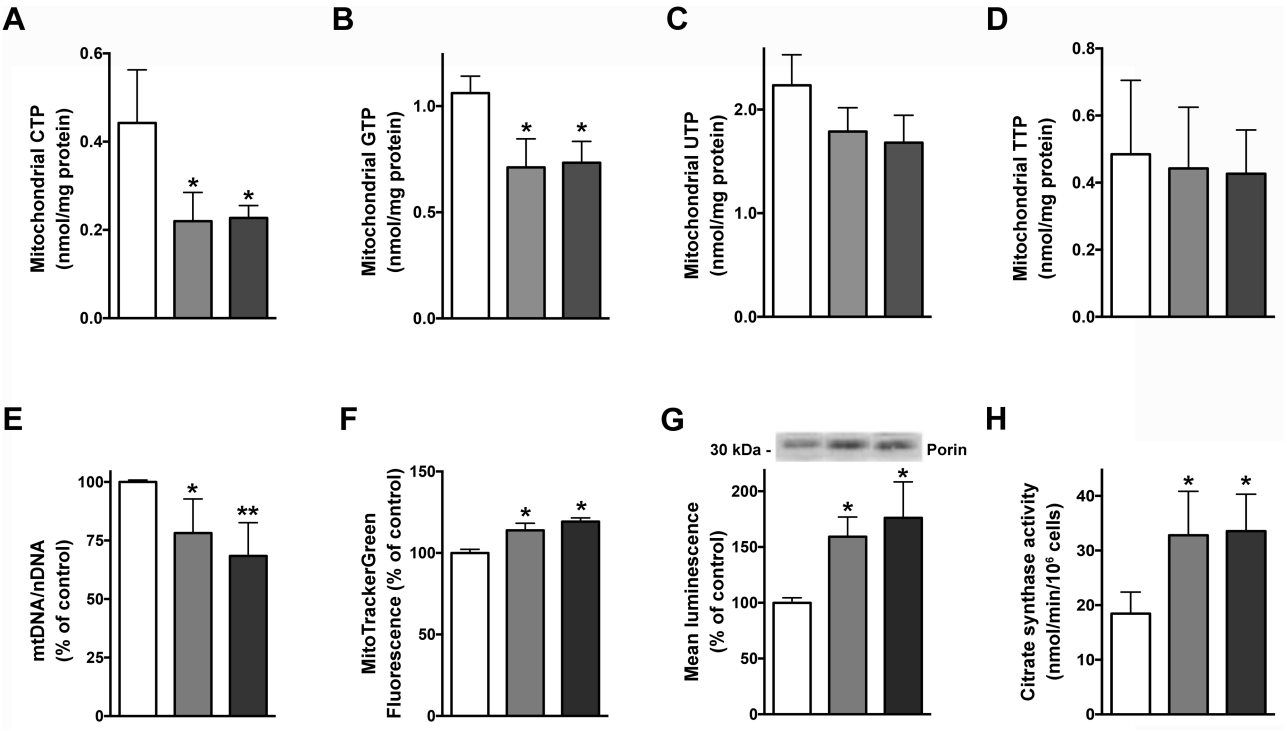

Figure 5. (A-D) Reduced mitochondrial CTP and GTP content in HeLa cells with downregulated *SLC25A36*. Mitochondria were isolated from LVshMM-HeLa (white column), LVshA36-HeLa.1 (gray column) and LVshA36-HeLa.2 (dark gray column) cells and nucleotide levels were determined by mass spectrometry. Data are the means ± SD of 3 independent preparations, *$P < 0.05$, one-way analysis with Bonferroni *t* test. (E-H) Reduced mtDNA content and increased mitochondrial mass in in HeLa cells with downregulated *SLC25A36*. (E) The mtDNA quantity relative to nuclear DNA was measured by real-time qRT PCR, as described in "Methods". Data are the means ± SD of 3 independent measurements, *$P < 0.05$, **$P < 0.01$, one-way analysis with Bonferroni *t* test. (F) Mitochondrial mass was estimated by marking LVshMM-HeLa, LVshA36-HeLa.1, and LVshA36-HeLa.2 cells with 250nM MitoTracker Green. Green fluorescence intensity of the probe was measured with Tali Image system. Data represent the means ± SD of 4 independent measurements, *$P < 0.05$, one-way analysis with Bonferroni *t* test. (G). Representative Western blot and densitometric analysis of LVshMM-HeLa (white column), LVshA36-HeLa.1 (gray column) and LVshA36-HeLa.2 (dark gray column) cell extracts blotted with an antibody against the mitochondrial Porin protein (Abcam UK, RRID:AB_10865182) revealed by enhanced chemiluminescence (Merck) on a ChemiDoc Touch Imaging System (BioRad). Histogram represents the means ± SD of 4 independent densitometric analyses, *$P < 0.05$, one-way analysis with Bonferroni *t* test. (H) Citrate synthase activity in LVshMM-HeLa (white column), LVshA36-HeLa.1 (gray column), and LVshA36-HeLa.2 cells (dark gray column). Histogram represents the means ± SD of 3 independent experiments performed with permeabilized cells (see methods), *$P < 0.05$, one-way analysis with Bonferroni *t* test.

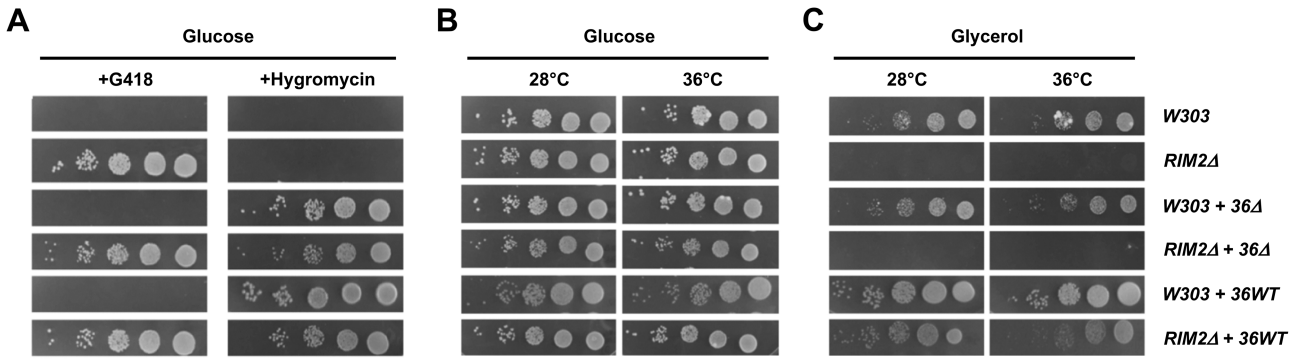

Figure 6. Complementation of *S. cerevisiae* RIM2Δ cells with wild-type *SLC25A36* or mutant *SLC25A36*. (A-C) Wild-type W303, W303 transformed with the wild-type *SLC25A36* or its mutated form, *RIM2*Δ and *RIM2*Δ transformed with the wild-type *SLC25A36* or its mutated form (shown as *WT*, *WT* + 36WT, *WT* + 36Δ, *RIM2*Δ, *RIM2*Δ + 36WT, *RIM2*Δ + 36Δ, respectively) haploid strains were selected on YPD with G-418 or Hygromycin (A) and spotted on solid YPD (B) or YPG (C) medium for 48 hours at 28 °C and at 36 °C as 4-fold serial dilution.

MCF-7 cells with downregulated SLC25A33 expressing PNC1 (15), was further confirmed in PNC2-downregulated HeLa cells by the increased expression of porin (Fig. 5G), a marker of the mitochondrial outer membrane, and by the enhanced activity of citrate synthase (Fig. 6H), a marker of the mitochondrial matrix, as compared with control. Altogether, these data point to an essential function for PNC2 in mitochondrial nucleotide transport and in the maintenance of mtDNA. Indeed, expression of either PNC1 or PNC2 was shown to suppress the growth defect of a yeast strain of *S. cerevisiae* devoid of *RIM2* (*RIM2Δ)*, its fungal orthologue (16) that loses mtDNA at very high frequency on nonfermentable carbon sources like glycerol (17).

To investigate whether mutated PNC2 can replace the Rim2p function, a *RIM2Δ* haploid strain was crossed with an isogenic wild-type haploid strain (W303) of the opposite mating type transformed with a plasmid containing either the wild-type *SLC25A36* (pl *36WT*) or its mutated form (pl *36Δ*), under the transcriptional control of the yeast *RIM2* promoter, so that during meiosis the mtDNA segregated in all 4 spores. After sporulation and tetrad analysis, the transformed W303 and *RIM2Δ*haploid strains were selected (Fig. 6A) and assayed for growth on either fermentable or nonfermentable carbon sources. The *RIM2Δ* strains transformed with either wild-type *SLC25A36* (*RIM2Δ* + *36WT*) or its mutated form (*RIM2Δ* + *36Δ*) grew equally well in the presence of glucose (Fig. 6B). By contrast, the *RIM2Δ* + *36Δ* cells were unable to grow in the presence of glycerol (Fig. 6C) due to loss of mtDNA (Fig. 7). The W303 strains containing endogenous wild-type *RIM2* could grow in both media irrespective of the plasmid used for transformation (Fig. 6B and 6C).

Discussion

This is the first report of a homozygous loss-of-function variant in SLC25A36 that causes hyperinsulinism/hyperammonemia syndrome. Human *SLC25A36* encodes PNC2, a protein that transports guanine and cytosine nucleotides across the inner mitochondrial membrane (3). We demonstrate that the newly identified pathogenic mutation leads to a 26-aa deletion in PNC2 and a strong impairment of its transport activity. We also provide evidence that PNC2 can regulate mitochondrial CTP and GTP levels, hence playing a key role in the homeostasis of mitochondrial (d)NTP pool, together with its close homologue, PNC1, encoded by the *SLC25A33* gene, which predominantly transports uridine and thymidine nucleotides (3, 14). Notably, both PNC1 and PNC2 have been found upregulated in mice lacking Mpv17, a mitochondrial inner membrane protein whose deficiency is associated with substantial decreases in the levels of dGTP and dTTP and severe mitochondrial DNA depletion (18, 19). The genome of *Drosophila melanogaster* contains only one gene with significant similarity to PNC1 and PNC2, named drim2. In keeping with the overlapping transport specificities and physiological roles of the human homologues, it has been shown that *D. melanogaster* S2R$^+$cells, silenced for drim2, contained markedly reduced pools of both purine and pyrimidine NTPs in mitochondria, whereas cytosolic pools were unaffected (20). Interestingly, drim2 homozygous knockout caused loss of mtDNA similarly to what was observed earlier following deletion of the yeast orthologue RIM2 (17). Here we show that PNC2 knockdown in HeLa cells leads to a significant reduction of mtDNA. Recently, Slc25a36 suppression was demonstrated to cause a decline of mtDNA also in mouse embryonic stem cells where PNC2 is required to maintain pluripotency (21). As previously observed in cells where PNC1 had been silenced (15) and cells with deficient Thymidine Kinase 2 (22), in PNC2-silenced HeLa cells the mitochondrial mass is increased (Fig. 6F-6H), displaying the same compensatory mechanism upon mtDNA level reduction due to altered mitochondrial nucleotide metabolism. These results also highlight the evolutionarily conserved role of this subfamily of homologous mitochondrial nucleotide transporters in mtDNA maintenance.

Inside mitochondria, GTP, beside taking part in several reactions like the succinylCoA synthetase reaction in the Krebs cycle, regulates the glutamic dehydrogenase (GDH) a key enzyme involved in insulin secretion from the pancreas (23), where we show that SLC25A36 is expressed at its utmost. In pancreatic β-cells, the combined activity of glycolysis and oxidative phosphorylation regulates ATP/ADP ratio, one of the key factors promoting insulin secretion. After glucose stimulation, ADP decrease inhibits ATP-sensitive K$^+$-channels (KATP channel), thus allowing the depolarization of the plasma membrane and Ca^{2+} influx in the cytosol, which is the main signal for the exocytosis of insulin (24, 25). However, additional metabolic signals are required to further support or amplify the insulin secretion, such as cAMP, NADPH, long chain acyl-CoA derivatives, and reactive oxygen species (ROS) (23). In this context, a key role is played by a

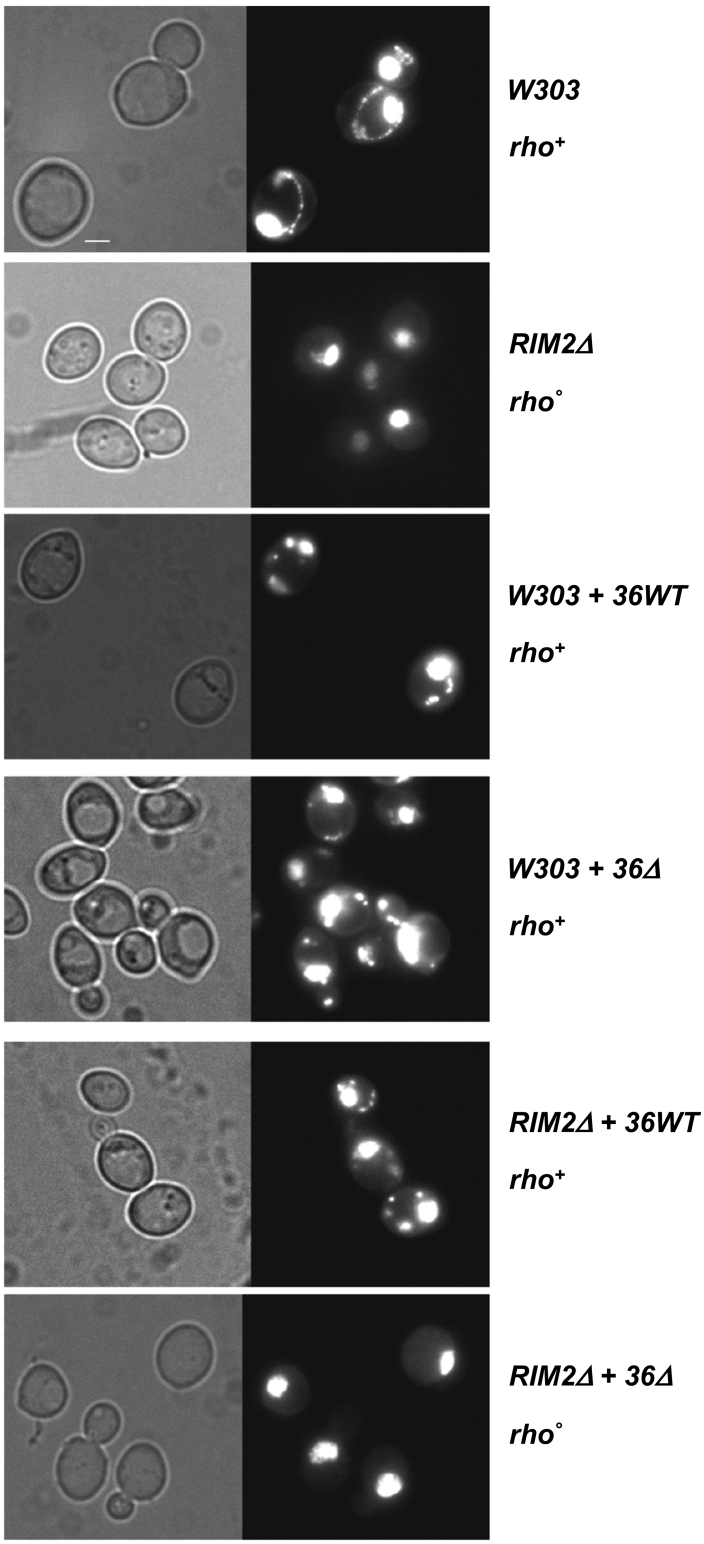

Figure 7. Mutant *SLC25A36* is unable to rescue mtDNA in *S. cerevisiae* RIM2 null mutants. Wild-type W303, W303 transformed with the wild-type *SLC25A36* or its mutated form RIM2Δ and RIM2Δ transformed the wild-type *SLC25A36* or its mutated form (shown as *WT, WT + 36WT, WT + 36Δ, RIM2Δ, RIM2Δ + 36WT, RIM2Δ + 36Δ,* respectively) haploid strains were grown until exponential phase in liquid YPD medium at 28 °C and stained with DAPI.

number of transporters of the inner mitochondrial membrane (26, 27). Downregulation of mitochondrial pyruvate carrier heterodimers MPC1 and MPC2 reduces glucose-stimulated insulin secretion in beta-cells, and in human and rat islets (28). Limited mitochondrial pyruvate oxidation also inhibits insulin secretion in islets from Mpc2Δ16 mice expressing a truncated MPC2 protein (29). Likewise, silencing of mitochondrial aspartate/glutamate carrier isoform 1

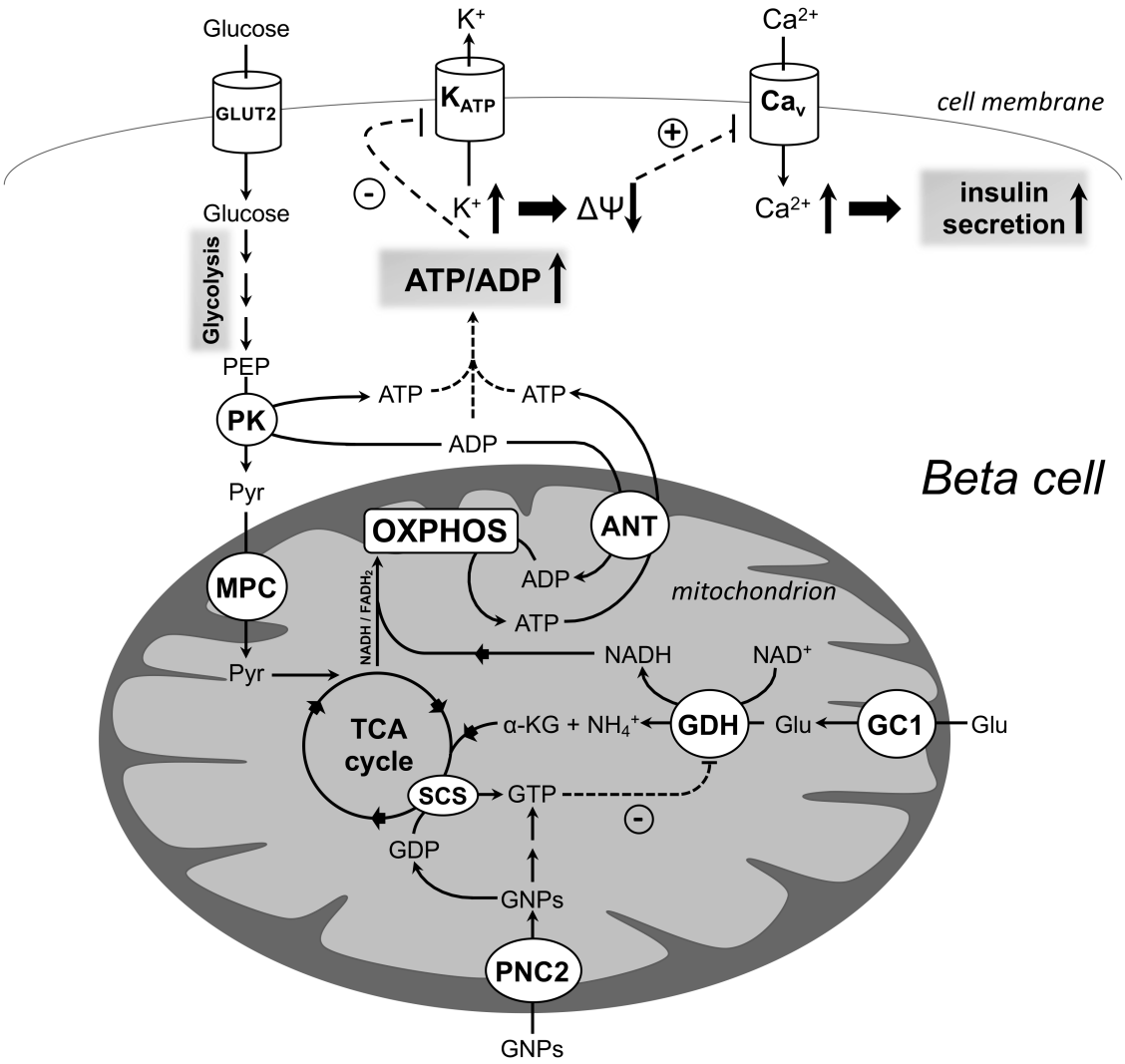

Figure 8. PNC2 as a new player in the regulation of insulin secretion. PNC2 catalyzes the transport of guanosine phosphates (GNPs) in exchange for other nucleotides across the inner mitochondrial membrane (3), thus feeding the mtGTP pool. In glucose-stimulated pancreatic beta-cells, a defective PNC2 may reduce mtGTP leading to an increase of glutamate oxidative deamination by glutamic dehydrogenase (GDH) and, consequently, a stimulation of TCA cycle activity and oxidative phosphorylation. The resulting increase in mitochondrial ATP exported out of the mitochondria by the adenine nucleotide translocator (ANT) in exchange with cytosolic ADP may further increase the high cytosolic ATP/ADP ratio due to the extra-mitochondrial pyruvate kinase (PK) activity (25). The massive reduction in cytosolic ADP closes KATP channels, thus intensifying the depolarization of the cell membrane and the increase in intracellular Ca^{2+} that triggers the exocytosis of insulin-containing vesicles. Abbreviations: Ca_v, voltage-dependent Ca^{2+}-channel; GC1 mitochondrial glutamate carrier isoform 1; GLUT2, glucose transporter isoform 2; K_{ATP}, K^+-ATP channel; MPC, mitochondrial pyruvate carrier; SCS, GTP-specific succinyl-CoA synthetase.

(AGC1) in insulinoma INS-1E cells reduced insulin exocytosis since glycolysis and, in turn, pyruvate oxidation is altered in the presence of impaired malate/aspartate NADH shuttle (30). Furthermore, the cataplerotic role of mitochondrial carriers for citrate (CIC), dicarboxylic acids (DIC) and for the oxoglutarate/malate exchange (OGC) is essential for the pyruvate-isocitrate cycling pathway that sustains the glucose-induced increase of cytosolic NADPH/$NADP^+$ ratio required for a correct insulin release (31-33).

Our results point to PNC2 as a new player in the regulation of the insulin secretion since we show here that its transport activity regulates mtGTP pool. Indeed, GTP is a potent allosteric inhibitor of the activity of GDH, an enzyme located in the mitochondrial matrix that plays an important role in insulin secretion (34). GDH catalyzes the reversible deamination of glutamate to 2-oxoglutarate with generation of NADH and is expressed in liver, kidney, brain, and pancreatic beta-cells. Missense dominant mutations of GDH that reduce the sensitivity of the enzyme to allosteric inhibition by GTP have been shown to cause the HI/HA syndrome (1).

The HI/HA syndrome is characterized by recurrent episodes of symptomatic hypoglycemia in combination with a persistent mild hyperammonemia (1, 2). Plasma ammonia levels are increased 3 to 5 times normal due to expression of mutant GDH in most HI/HA patients or due to PNC2/SLC25A36 deficiency in our patients, probably reflecting increased ammonia release from glutamate as well as impaired synthesis of N-acetylglutamate, a required allosteric activator of carbamoyl-phosphate synthetase, the rate-controlling first step in ammonia detoxification, due to reduction of substrate pool. Interestingly, it has been recently shown that the hyperammonemia associated with systemic activation of GDH originates from the kidney, rather than from the liver (35), where SLC25A36 is only poorly expressed.

In β-cells, where SLC25A36 is maximally expressed, enhanced glutamate oxidation can activate the triggering pathways of insulin release by raising the ATP/ADP ratio to cause closure of the KATP channel, opening the voltage-gated calcium channel and eventually raising cytosolic calcium. Our results indicate that the release of inhibitory control of GDH by mtGTP pool due to PNC2/SLC25A36 deficiency, leads to enhanced oxidative deamination of glutamate through GDH and excessive release of insulin (Fig. 8).

Accordingly, downregulation of the mitochondrial glutamate carrier (GC1) that catalyzes the transport of glutamate across the inner mitochondrial membrane reduces insulin exocytosis evoked by glucose stimulation (36). Of note, decrease of insulin secretory response has been observed in transgenic GDH knockout mice with reduced glutamate levels in the β-cells (37). This counterintuitive observation would rather fit with the less likely scenario of GDH operating in the direction of glutamate synthesis (37). The reductive amination of α-ketoglutarate catalyzed by GDH has been shown to operate in brain where glutamate formation would be important for ammonia fixation and a prerequisite for synthesis of glutamine during hyperammonemia (38), but the elucidation of the direction of the GDH reaction in different tissues/cells under different conditions is beyond the scope of this manuscript.

At variance with other forms of HI, the episodes of hypoglycemia occur in response to protein feeding in addition to fasting and may typically present as postprandial hypoglycemia (39). When protein catabolism is activated, leucine serves as an indicator of increased amino acid supply and stimulates insulin release by allosterically activating GDH. Normally, GDH activity is suppressed in the basal state by the potent inhibitory effects of GTP but gain-of-function GDH mutations (40) or PNC2/SLC25A36 deficiency (this study), which hamper the inhibitory effects of GTP, cause upregulation of leucine-stimulated insulin release and a constitutive oversecretion of insulin. High leucine concentration can occur following a high-protein feeding, which when precluded in 1 of the 2 patients with the adoption of a low-protein diet, strongly reduced the frequency of hypoglycemic attacks.

Acknowledgments

We wish to thank Riccardo Merafina (CNR-IBIOM) for technical assistance with functional studies. Imad Dweikat is now at the Faculty of Medicine, Arab American University, P2980106 Jenin, Palestine. Flora Guerra is now at the Department of Biological and Environmental Sciences and Technologies, Università del Salento, 73100 Lecce, Italy. Simona Todisco is now at the Department of Science, University of Basilicata, 85100 Potenza, Italy.

Financial Support

This study was partially supported by grants-in-aid from the University of Bari, "Fondi Ateneo 2016/8" and Ministero dell'Istruzione, dell'Università e della Ricerca (MIUR), Centre of Excellence "Genomics: genes involved in pathopysiological processes in the biomedical and agricultural fields" (CEGBA) (to L.P.) and from Consiglio Nazionale delle Ricerche (CNR), Flagship-project "Interomics" (to F.M.L. and L.P.).

Disclosures

The authors have nothing to disclose.

Data Availability

The exome FASTQ file is available upon request. All other data relevant to the study are included in the article.

References

1. MacMullen C, Fang J, Hsu BY, *et al.* Hyperinsulinism/hyperammonemia syndrome in children with regulatory mutations in the inhibitory guanosine triphosphate-binding domain of glutamate dehydrogenase. *J Clin Endocrinol Metab.* 2001;86(4):1782-1787.
2. Stanley CA. Hyperinsulinism/hyperammonemia syndrome: insights into the regulatory role of glutamate dehydrogenase in ammonia metabolism. *Mol Genet Metab.* 2004;81(Suppl 1):S45-S51.
3. Di Noia MA, Todisco S, Cirigliano A, *et al.* The human SLC25A33 and SLC25A36 genes of solute carrier family 25 encode two mitochondrial pyrimidine nucleotide transporters. *J Biol Chem.* 2014;289(48):33137-33148.
4. Palmieri F, Monné M. Discoveries, metabolic roles and diseases of mitochondrial carriers: a review. *Biochim Biophys Acta.* 2016;1863(10):2362-2378.
5. Nishimura M, Suzuki S, Satoh T, Naito S. Tissue-specific mRNA expression profile of human solute carrier 35 transporters. *Drug Metab Pharmacokinet.* 2009;24(1):91-99.
6. Bustin SA. Absolute quantification of mRNA using real-time reverse transcription polymerase chain reaction assays. *J Mol Endocrinol.* 2000;25(2):169-193.
7. Palmieri F, Indiveri C, Bisaccia F, Iacobazzi V. Mitochondrial metabolite carrier proteins: purification, reconstitution, and transport studies. *Methods Enzymol.* 1995;260:349-369.
8. Yuan B, Latek R, Hossbach M, Tuschl T, Lewitter F. siRNA Selection Server: an automated siRNA oligonucleotide prediction server. *Nucleic Acids Res.* 2004;32(Web Server issue):W130-W134.
9. Profilo E, Peña-Altamira LE, Corricelli M, *et al.* Down-regulation of the mitochondrial aspartate-glutamate carrier isoform 1 AGC1 inhibits proliferation and N-acetylaspartate synthesis in Neuro2A cells. *Biochim Biophys Acta.* 2017;1863(6):1422-1435.
10. Vozza A, Parisi G, De Leonardis F, *et al.* UCP2 transports C4 metabolites out of mitochondria, regulating glucose and glutamine oxidation. *Proc Natl Acad Sci USA.* 2014;111(3):960-965.
11. Xing J, Apedo A, Tymiak A, Zhao N. Liquid chromatographic analysis of nucleosides and their mono-, di- and triphosphates using porous graphitic carbon stationary phase coupled with electrospray mass spectrometry. *Rapid Commun Mass Spectrom.* 2004;18(14):1599-1606.
12. Gasparre G, Porcelli AM, Bonora E, *et al.* Disruptive mitochondrial DNA mutations in complex I subunits are markers of oncocytic phenotype in thyroid tumors. *Proc Natl Acad Sci USA.* 2007;104(21):9001-9006.
13. Amati-Bonneau P, Valentino ML, Reynier P, *et al.* () OPA1 mutations induces mitochondrial DNA instability and optic atrophy "plus" phenotypes. *Brain.* 2008;131(Pt2):338-351.
14. Floyd S, Favre C, Lasorsa FM, *et al.* The insulin-like growth factor-I-mTOR signaling pathway induces the mitochondrial pyrimidine nucleotide carrier to promote cell growth. *Mol Biol Cell.* 2007;18(9):3545-3555.
15. Favre C, Zhdanov A, Leahy M, Papkovsky D, O'Connor R. Mitochondrial pyrimidine nucleotide carrier (PNC1) regulates mitochondrial biogenesis and the invasive phenotype of cancer cells. *Oncogene.* 2010;29(27):3964-76.

16. Marobbio CM, Di Noia MA, Palmieri F. Identification of a mitochondrial transporter for pyrimidine nucleotides in Saccharomyces cerevisiae: bacterial expression, reconstitution and functional characterization. *Biochem J*. 2006;393(Pt2):441-446.
17. Van Dyck E, Jank B, Ragnini A, *et al*. Overexpression of a novel member of the mitochondrial carrier family rescues defects in both DNA and RNA metabolism in yeast mitochondria. *Mol Gen Genet*. 1996;246(4):426-436.
18. Dalla Rosa I, Cámara Y, Durigon R, *et al*. MPV17 loss causes deoxynucleotide insufficiency and slow DNA replication in mitochondria. *PLoS Genet*. 2016;12(1):e1005779.
19. Bottani E, Giordano C, Civiletto G, *et al*. AAV-mediated liver-specific MPV17 expression restores mtDNA levels and prevents diet-induced liver failure. *Mol Ther*. 2014;22(1):10-17.
20. Da-Rè C, Franzolin E, Biscontin A, *et al*. Functional characterization of drim2, the Drosophila melanogaster homolog of the yeast mitochondrial deoxynucleotide transporter. *J Biol Chem*. 2014;289(11):7448-7459.
21. Xin Y, Wang Y, Zhong L, Shi B, Liang H, Han J. Slc25a36 modulates pluripotency of mouse embryonic stem cells by regulating mitochondrial function and glutathione level. *Biochem J*. 2019;476(11):1585-1604.
22. Zhou X, Kannisto K, Curbo S, *et al*. Thymidine kinase 2 deficiency-induced mtDNA depletion in mouse liver leads to defect β-oxidation. *PLoS One*. 2013;8(3):e58843.
23. Maechler P. Glutamate pathways of the beta-cell and the control of insulin secretion. *Diabetes Res Clin Pract*. 2017;131:149-153.
24. Wilson DF, Cember ATJ, Matschinsky FM. The thermodynamic basis of glucose-stimulated insulin release: a model of the core mechanism. *Physiol Rep*. 2017;5(12):e13327.
25. Lewandowski SL, Cardone RL, Foster HR, *et al*. Pyruvate kinase controls signal strength in the insulin secretory pathway. *Cell Metab*. 2020;32(5):736-750.e5.
26. Brun T, Scarcia P, Li N, *et al*. Changes in mitochondrial carriers exhibit stress-specific signatures in INS-1Eβ-cells exposed to glucose versus fatty acids. *PLoS One*. 2013;8(12):e82364.
27. Brun T, Maechler P. Beta-cell mitochondrial carriers and the diabetogenic stress response. *Biochim Biophys Acta*. 2016;1863(10):2540-2549.
28. Patterson JN, Cousteils K, Lou JW, Manning Fox JE, MacDonald PE, Joseph JW. Mitochondrial metabolism of pyruvate is essential for regulating glucose-stimulated insulin secretion. *J Biol Chem*. 2014;289(19):13335-13346.
29. Vigueira PA, McCommis KS, Schweitzer GG, *et al*. Mitochondrial pyruvate carrier 2 hypomorphism in mice leads to defects in glucose-stimulated insulin secretion. *Cell Rep*. 2014;7(6):2042-2053.
30. Casimir M, Rubi B, Frigerio F, Chaffard G, Maechler P. Silencing of the mitochondrial NADH shuttle component aspartate-glutamate carrier AGC1/Aralar1 in INS-1E cells and rat islets. *Biochem J*. 2009;424(3):459-466.
31. Joseph JW, Jensen MV, Ilkayeva O, *et al*. The mitochondrial citrate/isocitrate carrier plays a regulatory role in glucose-stimulated insulin secretion. *J Biol Chem*. 2006;281(47):35624-35632.
32. Huypens P, Pillai R, Sheinin T, *et al*. The dicarboxylate carrier plays a role in mitochondrial malate transport and in the regulation of glucose-stimulated insulin secretion from rat pancreatic beta cells. *Diabetologia*. 2011;54(1):135-145.
33. Odegaard ML, Joseph JW, Jensen MV, *et al*. The mitochondrial 2-oxoglutarate carrier is part of a metabolic pathway that mediates glucose- and glutamine-stimulated insulin secretion. *J Biol Chem*. 2010;285(22):16530-16537.
34. Stanley CA, Lieu YK, Hsu BY, *et al*. Hyperinsulinism and hyperammonemia in infants with regulatory mutations of the glutamate dehydrogenase gene. *N Engl J Med*. 1998;338(19):1352-1357.
35. Treberg JR, Clow KA, Greene KA, Brosnan ME, Brosnan JT. Systemic activation of glutamate dehydrogenase increases renal ammoniagenesis: implications for the hyperinsulinism/hyperammonemia syndrome. *Am J Physiol Endocrinol Metab*. 2010;298(6):E1219-E1225.
36. Casimir M, Lasorsa FM, Rubi B, *et al*. Mitochondrial glutamate carrier GC1 as a newly identified player in the control of glucose-stimulated insulin secretion. *J Biol Chem*. 2009;284(37):25004-25014.
37. Carobbio S, Frigerio F, Rubi B, *et al*. Deletion of glutamate dehydrogenase in beta-cells abolishes part of the insulin secretory response not required for glucose homeostasis. *J Biol Chem*. 2009;284(2):921-929.
38. Voss CM, Arildsen L, Nissen JD, *et al*. Glutamate dehydrogenase is important for ammonia fixation and amino acid homeostasis in brain during hyperammonemia. *Front Neurosci*. 2021;15:646291.
39. Hsu BY, Kelly A, Thornton PS, Greenberg CR, Dilling LA, Stanley CA. Protein-sensitive and fasting hypoglycemia in children with the hyperinsulinism/hyperammonemia syndrome. *J Pediatr*. 2001;138(3):383-389.
40. Kelly A, Ng D, Ferry RJ Jr, *et al*. Acute insulin responses to leucine in children with the hyperinsulinism/hyperammonemia syndrome. *J Clin Endocrinol Metab*. 2001;86(8):3724-3728.